

Global sensitivity analysis informed model reduction and selection applied to a Valsalva maneuver model

E. Benjamin Randall^{a,c,*}, Nicholas Z. Randolph^{b,c}, Alen Alexanderian^c, Mette S. Olufsen^{c,**}

^aDepartment of Molecular and Integrative Physiology, University of Michigan, Ann Arbor, MI

^bDepartment of Bioinformatics and Computational Biology, University of North Carolina at Chapel Hill, Chapel Hill, NC

^cDepartment of Mathematics, North Carolina State University, Raleigh, NC

Abstract

In this study, we develop a methodology for model reduction and selection informed by global sensitivity analysis (GSA) methods. We apply these techniques to a control model that takes systolic blood pressure and thoracic tissue pressure data as inputs and predicts heart rate in response to the Valsalva maneuver (VM). The study compares four GSA methods based on Sobol' indices (SIs) quantifying the parameter influence on the difference between the model output and the heart rate data. The GSA methods include standard scalar SIs determining the average parameter influence over the time interval studied and three time-varying methods analyzing how parameter influence changes over time. The time-varying methods include a new technique, termed limited-memory SIs, predicting parameter influence using a moving window approach. Using the limited-memory SIs, we perform model reduction and selection to analyze the necessity of modeling both the aortic and carotid baroreceptor regions in response to the VM. We compare the original model to systematically reduced models including (i) the aortic and carotid regions, (ii) the aortic region only, and (iii) the carotid region only. Model selection is done quantitatively using the Akaike and Bayesian Information Criteria and qualitatively by comparing the neurological predictions. Results show that it is necessary to incorporate both the aortic and carotid regions to model the VM.

Keywords: Mathematical modeling, Sobol' indices, Time-dependent processes, Akaike Information Criterion, Bayesian Information Criterion

Abbreviations (alphabetically)

Akaike information criterion with correction	AICc
Bayesian information criterion	BIC
Delay differential equations	DDE
Electrocardiogram	ECG
Generalized Sobol' indices	GSIs
Global sensitivity analysis	GSA
Initial conditions	ICs
Intrathoracic pressure	ITP
Limited-memory Sobol' indices	LMSIs
Local sensitivity analysis	LSA
Ordinary differential equations	ODEs
Piecewise cubic Hermite interpolating polynomial	PCHIP
Pointwise-in-time Sobol' indices	PTSIs
Quantity of interest	QoI
Respiratory sinus arrhythmia	RSA
Sobol' indices	SIs
Systolic blood pressure	SBP
Valsalva maneuver	VM

1. Introduction

Mathematical models describing cardiovascular processes are typically complex with nonlinear interactions. They have many interrelated states and a large number of parameters. Reducing these models may help model-based data analysis provided that the reduced model retains similar behavior to the original. Several formal model reduction methods exist [3] but most focus on analyzing input-output relationships, ignoring predicted quantities. Moreover, they typically identify one reduced model when in fact many can arise. We develop a systematic approach for model reduction and selection via global sensitivity analysis. We then apply this protocol to our model [26] that takes systolic blood pressure (SBP) and intrathoracic tissue pressure (ITP) as inputs to predict the heart rate response to the Valsalva maneuver (VM), characterized by forceful exhalation against a resistance. Moreover, we use model selection to investigate whether differentiating between the aortic and carotid baroreceptor afferent signals is necessary for accurate prediction of heart rate.

To analyze parameter influence on a quantity of interest (QoI), we employ *local* (LSA) or *global* (GSA) sensitivity analysis. LSA (e.g., [6, 20, 23]) computes partial derivatives of the QoI with respect to the nominal parameter values, whereas GSA [30] computes parameter influence by analyzing parameters and their interactions over the entire parameter space. Here,

*Corresponding author

**Principal corresponding author

Email addresses: ebrandal@umich.edu (E. Benjamin Randall), nrandol@unc.edu (Nicholas Z. Randolph), aalexan3@ncsu.edu (Alen Alexanderian), msolufse@ncsu.edu (Mette S. Olufsen)

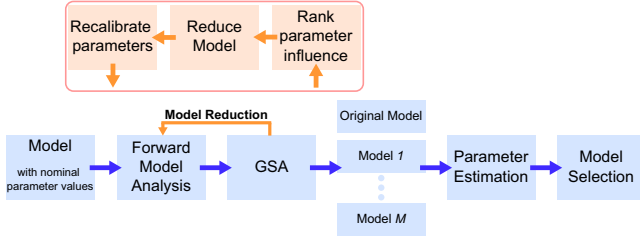


Figure 1: Workflow diagram illustrating the procedure outlined in Section 2. From left to right: A model is developed and nominal parameter values, i.e., the values that provide the initial model prediction, are determined. Forward model analysis produces outputs which undergo global sensitivity analysis (GSA). The GSA results are used to reduce the model (orange arrow), producing M reduced models. For each model, a subset of parameters is estimated to fit data. The reduced model that captures the original model best, qualitatively and quantitatively, is selected. *Model Reduction Step* (insert): Using GSA, parameters are ranked from most to least influential, and parameters below a preset threshold are termed noninfluential. These parameters are “removed” by fixing them at their nominal values or analytically excising the model components associated with them. For each reduced model, nominal parameter values are recalibrated and estimated, and GSA is performed again.

“nominal” refers to the *a priori* guess and/or calculation used to compute the initial model prediction (before parameter estimation). Popular methods include Sobol’ indices (SIs) [29, 33] (used here), Morris screening [21, 22], generalized sensitivity functions [13], and moment-independent importance measures [12]. Morris screening is computationally inexpensive but does not account for higher order interactions. Generalized sensitivity functions characterize model sensitivity to nominal parameter values and take into account parameter interactions, yet make stringent assumptions on local parameter identifiability. Moment-independent importance measures focus on constructing probability density functions that are computationally expensive and intractable for high dimensional systems.

We compute our GSA using SIs due to their wide usage and applicability [5, 14, 17, 36]. SIs apportion relative contributions of the effect on the QoI to each parameter. Originally developed to analyze parameter influence in models with scalar outputs [33] (*scalar* SIs), they have recently been extended to analyze time-varying QoIs [1]. *Pointwise-in-time* Sobol’ indices (PT-SIs) calculate the SI at every time point but do not account for the changes in the pointwise variance over time [2, 14]. To incorporate time dependence, *generalized* Sobol’ indices (GSIs) integrate the pointwise variance over a specified time interval [1, 7]. However, for processes that involve significant, short-lived disturbances to the steady-state behavior, integration over the entire time interval diminishes the effect of features that play a transient role. We illustrate this point using our VM model [26], where the breath hold causes a significant and fast model response. To mitigate this issue, we introduce *limited-memory* Sobol’ indices (LMSIs) that account for parameter interactions and the time history of the variance by applying weights from a moving window.

We also propose a methodology for model reduction and selection. For model reduction, we use the LMSIs to select parameters that are noninfluential over the time interval. These parameters are “removed” by (i) excision of the equation(s) as-

sociated with them [6, 19] or (ii) fixing the them at their nominal values [33]. This process generates a set of reduced models upon which we perform model selection using the Akaike Information Criterion with correction (AICc) and Bayesian Information Criterion (BIC) [37]. Finally, we determine if the reduced models can predict heart rate and autonomic VM responses similar to the original model.

The new contributions of this article include: (i) the development of LMSIs for time-dependent processes to analyze our model’s [26] response to the VM; and (ii) a GSA-informed model reduction and selection protocol. We use model selection to test whether it is necessary to include afferent signaling from the carotid region only, the aortic region only, or both regions simultaneously to predict heart rate dynamics and neural tones.

2. Methods

Figure 1 depicts the model reduction and selection workflow, which includes the following components:

1. *Forward model analysis*: We consider the QoI, which is the time-varying residual vector

$$\mathbf{r}(t_j; \theta) = \frac{H(t_j; \theta) - H_d(t_j)}{H_d(t_j)} \quad (1)$$

where $H(t_j; \theta)$ denotes the heart rate model output at time t_j for $j = 1, \dots, N$ and $H_d(t_j)$ the corresponding heart rate data. Model predictions depend on the parameter vector $\theta \in \Omega_p \subseteq \mathbb{R}^p$, for Ω_p the parameter space of dimension p .

2. *Global sensitivity analysis*: To determine parameter influence on the QoI, we compute scalar SIs with respect to

$$\|\mathbf{r}(t; \theta)\|_2 = \left(\sum_{j=1}^N \mathbf{r}(t_j; \theta)^2 \right)^{1/2} \quad (2)$$

as well as the time-varying PTSIs, GSIs, and LMSIs with respect to \mathbf{r} .

- (a) *Parameter influence* is computed with the chosen index. We compute LMSIs to determine noninfluential parameters having an index below a given threshold.
- (b) *Model reduction* “removes” noninfluential parameters by fixing them at their nominal values or analytically removing equations associated with them.
- (c) *Model recalibration* ensures that the reduced model produces similar predictions as the original.
- (d) *GSA on the reduced model* is conducted to test if all parameters are influential. This step is necessary since model reduction can change the relative ranking of parameter influence and result in some parameters becoming noninfluential.

Steps (b)-(d) are repeated iteratively until the system has no noninfluential parameters. At any point, there may be cases where one could remove one parameter over another, creating branches of reduced models.

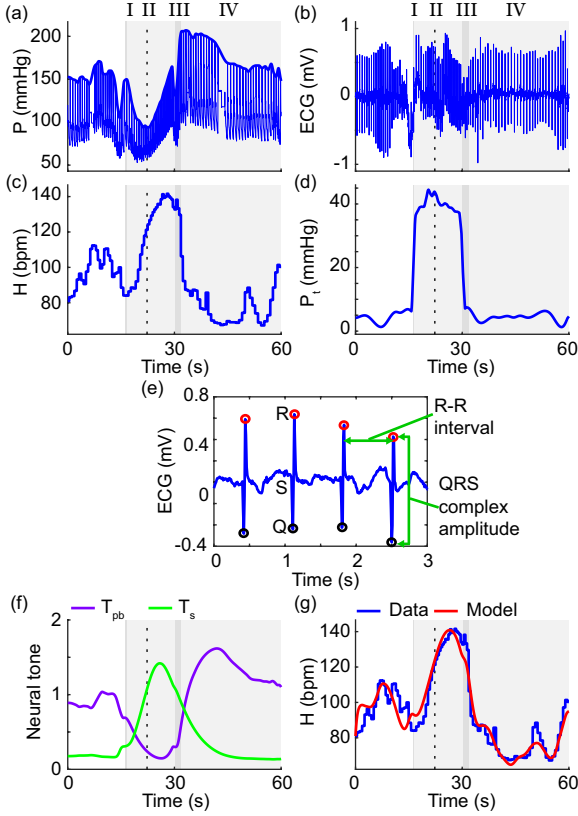


Figure 2: Valsalva maneuver (VM) for a representative subject. The VM phases are represented as alternating gray (I and III) and light gray (II and IV) boxes. Phase II is divided into early and late stages (vertical dotted black line). Phases: I. Initiation of the breath hold causes a sharp increase in blood pressure (P , mmHg) and a decrease in heart rate (H , bpm). Early II. P drops and H accelerates. Late II. H accelerates further, which increases P . III. Release of the breath hold causes a sharp drop in P . IV. P overshoots and H undershoots, both returning to baseline within 30 s. (a) P with systolic blood pressure (bold) indicated. (b) Electrocardiogram (ECG, mV). (c) H . (d) Thoracic pressure (P_t , mmHg, equation (A.7)). (e) ECG zoom with Q (black circles), R (red circles), and S waves indicated. Green arrows show the amplitude of the QRS-complex (the set of Q, R, and S waves) and the R-R interval (the time between two consecutive R waves). (f) Baroreflex-mediated parasympathetic (T_{pb} , dimensionless, purple) and sympathetic (T_s , dimensionless, green) neural tones. (g) Heart rate model output (H , bpm, red) fitted to data (blue). Optimized parameter values for panels f and g are listed in Table 1.

3. *Reduced models*: We create a set $\mathcal{M} = \{m_0, m_1, \dots, m_M\}$ for m_0 the original model and m_k the reduced models for $k = 1, \dots, M$.
4. *Parameter estimation*: To determine an identifiable parameter subset ($\hat{\theta}$), we use subset selection [19, 22, 23, 24], which is local in nature, since the model is evaluated at specific parameter values. Each reduced model is fitted to data, estimating $\hat{\theta}$ by minimizing the least squares error.
5. *Model selection*: To ensure that the reduced models produce outputs within physiological ranges, we perform model selection both quantitatively and qualitatively. Quantitatively, we analyze goodness of fit by calculating relative AICc and BIC values. Qualitatively, we assume the original model is the true signal and analyze the predicted neural tones of the reduced models.

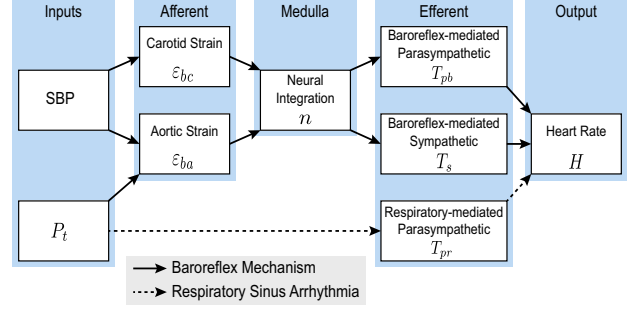


Figure 3: Model diagram reproduced from [26]. Systolic blood pressure (SBP, mmHg, Figure 2a) and thoracic pressure (P_t , mmHg, Figure 2d, equation (A.7)) are inputs. *Baroreflex pathway*: (solid arrows) Carotid baroreceptor strain (ε_{bc} , dimensionless, equation (A.1)) depends on SBP only and aortic strain (ε_{ba} , dimensionless, equation (A.2)) depends on SBP and P_t . They are integrated in the medulla (n , s^{-1} , equation (8)), which initiates a dynamic change in baroreflex-mediated parasympathetic (T_{pb} , dimensionless, equation (A.3)) and sympathetic (T_s , dimensionless, equation (A.4)) tones. *Respiratory sinus arrhythmia (RSA) pathway*: (dotted arrows) RSA depends solely on P_t that modulates the RSA-mediated parasympathetic tone (T_{pr} , dimensionless, equation (A.5)). All efferent outflows combine to control heart rate (H , bpm, equation (9)).

2.1. The Valsalva maneuver

The VM is a clinical test involving forced expiration against a closed airway while maintaining an open glottis [9]. It stimulates the autonomic nervous system via the baroreflex in response to blood pressure changes in the aortic arch and the carotid sinus. The body responds to a sudden decrease in blood pressure, causing compensatory responses in heart rate to restore blood pressure to baseline. Figure 2 displays a representative VM and includes the four VM phases.

2.2. Data acquisition and processing

The data is from a 21-year-old healthy female following our previous work [26]. Figure 2 displays the electrocardiogram (ECG), blood pressure, and heart rate. SBP (Figure 2a) is obtained by interpolating the local maxima of consecutive blood pressure waveforms using a piecewise cubic Hermite interpolating polynomial (PCHIP). Similarly, we construct a respiration signal from the ECG (Figure 2b) using PCHIP to detect amplitudes of the QRS complexes (sets of Q, R, and S waves in the ECG) (Figure 2e). Figure 2d plots thoracic pressure (P_t , equation (A.7)) during the VM. Heart rate (Figure 2c) is computed from the ECG by detecting R-R intervals, the time between two consecutive R waves (Figure 2e).

2.3. Model development

The model is a system of stiff ordinary (ODEs) and delay (DDEs) differential equations with 6 states and 25 parameters that takes SBP and ITP as inputs to predict heart rate, H , in response to a VM. Figure 3 displays the model schematic with the baroreflex (solid arrows) and respiratory sinus arrhythmia (RSA, dotted arrows) pathways. The model is of the form

$$\frac{d\mathbf{x}(t)}{dt} = f(t, \mathbf{x}(t), \mathbf{x}(t-D_s); \theta), \quad \mathbf{x}(t) = \mathbf{x}_0 \text{ for } t \in [-D_s, 0]. \quad (3)$$

Here, $\mathbf{x}(t) = [\varepsilon_{bc}(t), \varepsilon_{ba}(t), T_{pb}(t), T_{pr}(t), T_s(t), H(t)]^T \in \mathbb{R}^6$, where ε_{bc} and ε_{ba} are the carotid and aortic baroreceptor strains,

Table 1: Description of the model parameters and units. Nominal (Nom) values, lower (LB) and upper (UB) bounds, along with an explanation for the chosen bounds. Optimized (Opt) parameters for the model outputs in Figure 2f and 2g are listed in the last column.

Symbol	Units	Nom	LB	UB	Explanation	Opt
<i>Offset</i>						
A		5	2.5	7.5	Nom \pm 50%	
<i>Convex parameter</i>						
B	s ⁻¹	0.5	0.01	1	[0, 1]	0.43*
<i>Afferent and efferent gains</i>						
K _b		0.1	0.05	0.15	Nom \pm 50%	
K _{pb}		5	2.5	7.5	Nom \pm 50%	
K _{pr}		1	0.5	1.5	Nom \pm 50%	
K _s		5	2.5	7.5	Nom \pm 50%	
<i>Time-scales</i>						
τ_b	s	0.9	0.45	1.35	Nom \pm 50%	
τ_{pb}	s	6.5	0.01	17.9	Mean \pm 2SD	4.26*
τ_{pr}	s	9.6	0.01	31.2	Mean \pm 2SD	2.75*
τ_s	s	10	5	15	Nom \pm 50%	
τ_H	s	0.5	0.25	0.75	Nom \pm 50%	
<i>Sigmoid steepnesses</i>						
q _w	mmHg ⁻¹	0.04	0.02	0.06	Nom \pm 50%	
q _{pb}	s	10	5	15	Nom \pm 50%	
q _{pr}	mmHg ⁻¹	1	0.5	1.5	Nom \pm 50%	
q _s	s	10	5	15	Nom \pm 50%	
<i>Half-saturation values</i>						
s _w	mmHg	123	83	163	Mean \pm 2SD	149**
s _{pb}	s ⁻¹	0.54	0.53	0.55	Mean \pm 2SD	0.54**
s _{pr}	mmHg	4.88	4.46	5.3	Mean \pm 2SD	4.50**
s _s	s ⁻¹	0.05	0.04	0.06	Mean \pm 2SD	
<i>Heart rate gains</i>						
H _I	bpm	100	86	114	Mean \pm 2SD	106**
H _{pb}		0.5	0.1	0.9	Mean \pm 2SD	0.44*
H _{pr}		0.3	0.01	1.1	Mean \pm 2SD	0.48*
H _s		0.3	0.01	1.1	Mean \pm 2SD	0.28*
<i>VM start and end</i>						
t _s	s	data				16.2**
t _e	s	data				30.2**
<i>Delay ***</i>						
D _s	s	3				

SD - standard deviation. VM - Valsalva maneuver.

A blank space in the Units column indicates that the parameter is dimensionless.

A blank space in the Opt column indicates that the parameter is not estimated, i.e., it is kept at its nominal value.

* The parameter was optimized to fit the data.

** The parameter was calculated from data.

*** D_s is included in the model but not analyzed. This parameter is held fixed at its nominal value.

respectively, T_{pb} and T_s are the baroreflex-mediated parasympathetic and sympathetic tones, respectively, and T_{pr} is the RSA-mediated parasympathetic tone. $f : \mathbb{R}^{1+2(6)+25} \rightarrow \mathbb{R}^6$ is the right hand side of the system, \mathbf{x}_0 is the vector of initial conditions, D_s $\in \mathbb{R}$ (s) is the discrete delay, and $\theta \in \mathbb{R}^{25}$ is a vector of parameters, including

$$\theta = [A, B, K_b, K_{pb}, K_{pr}, K_s, \tau_b, \tau_{pb}, \tau_{pr}, \tau_s, \tau_H, q_w, q_{pb}, q_{pr}, q_s, s_w, s_{pb}, s_{pr}, s_s, H_I, H_{pb}, H_{pr}, H_s, t_s, t_e]^T. \quad (4)$$

Table 1 lists the nominal parameter values. All states except T_s and H are modeled as a first-order linear equation of the form

$$\frac{dx}{dt} = \frac{-x(t) + K_x G_x(t)}{\tau_x}, \quad (5)$$

where x is a state, K_x is the gain, G_x is a nonlinear function, and τ_x is the time-scale. For ε_{bc} and ε_{ba} , G_x(t) takes the form

$$G_{bj}(t) = 1 - \sqrt{\frac{1 + e^{-q_w(P_j(t)-s_w)}}{A + e^{-q_w(P_j(t)-s_w)}}} \quad (6)$$

for j = c or a for carotid or aortic, respectively, where P_j denotes the pressure input, A (dimensionless) is an offset parameter, and q_w (mmHg⁻¹) and s_w (mmHg) are the steepness and half-saturation values. For T_{pb} and T_s, G_x(t) takes the form

$$G_l(t) = \frac{1}{1 + e^{q_l(n(t)-s_l)}} \quad (7)$$

for l = pb and s for baroreflex-mediated parasympathetic and sympathetic, respectively, where q_l (s) and s_l (s⁻¹) are the steepness and half-saturation values, respectively, and

$$n(t) = B(G_{bc}(t) - \varepsilon_{bc}(t)) + (1 - B)(G_{ba}(t) - \varepsilon_{ba}(t)) \quad (8)$$

for B $\in [0, 1]$ (s⁻¹). Figure 2f shows the optimized model predictions for T_{pb} and T_s. For T_{pr}, G_x(t) takes a similar form as equation (7), but the time-varying input is P_t (equation (A.7)). Lastly, H is determined by the ODE

$$\frac{dH(t)}{dt} = \frac{-H(t) + \tilde{H}(t)}{\tau_H}, \quad (9)$$

where τ_H (s) is a time-scale and

$$\tilde{H}(t) = H_I(1 - H_{pb}T_{pb}(t) + H_{pr}T_{pr}(t) + H_sT_s(t)). \quad (10)$$

H_I (bpm) is the intrinsic heart rate, whereas H_{pb}, H_{pr}, and H_s are dimensionless gains. The model equations are summarized in Appendix A. Figure 2g shows the optimized model fit to data.

Initial condition calculations are in Appendix B. The model is solved using the stiff DDE solver RADAR5 [8] with relative and absolute tolerances of 10⁻⁸. As described in Appendix C, H was fitted to the heart rate data by estimating a parameter subset ($\hat{\theta}$, equation (C.3)) that minimizes the least squares error (J, equation (C.4)) between the model output and the data. The GSA and parameter estimation are performed on the logarithm of the parameters. We assume that the logarithm of each parameter is uniformly distributed between the logarithm of their respective parameter ranges, given in Table 1. The data and run-time environment can be found in [28].

Upper and lower parameter bounds are given in Table 1. Parameters not calculated *a priori* are varied $\pm 50\%$ of their nominal values. Parameters calculated from data have bounds set to the mean ± 2 SD. To prevent negative parameter values, we set the lower bound to 0.01 where necessary. The parameter B varies from 0 to 1. The parameter τ_s is an exception since it interacts with D_s and can cause instability [27]. Hence, τ_s is varied $\pm 50\%$ of its nominal value to remain stable.

2.4. Global sensitivity analysis

We use variance-based SIs [29, 33] for the GSA. This section discusses four different methods for computing SIs: scalar [29], pointwise-in-time [2], generalized [1], and limited-memory (new). A reference table of symbols is compiled in Table 2.

Table 2: Summary of Sobol' index (SI) symbols.

SI Type	Symbol		Reference
	Main Effect	Total Effect	
Scalar	$\mathcal{S}_i(f)$	$\mathcal{T}_i(f)$	[29]
PTSIs	$\mathcal{S}_i(f; t)$	$\mathcal{T}_i(f; t)$	[2]
GSIs	$\mathcal{S}_i(f; [0, t])$	$\mathcal{T}_i(f; [0, t])$	[1]
LMSIs	$\mathcal{S}_i(f; [t - \Delta, t])$	$\mathcal{T}_i(f; [t - \Delta, t])$	This study

PTSIs - pointwise-in-time Sobol' indices.

GSIs - generalized Sobol' indices.

LMSIs - limited-memory Sobol' indices.

$i = 1, \dots, p$ denotes the parameter index.

2.4.1. Scalar Sobol' indices

Consider a mathematical model f with a scalar output y dependent on $\theta \in \Omega_p \subseteq \mathbb{R}^p$, a random vector of p statistically independent model parameters with a uniform distribution spanning Ω_p ; that is, $y = f(\theta)$. For each parameter θ_i , we compute its contribution to the variance of y [32, 33]. Assuming parameter independence, the main effect on f due to θ_i is

$$\mathcal{S}_i(f) = \frac{\mathbb{V}_{\theta_i}(\mathbb{E}_{\theta_{-i}}[f|\theta_i])}{\mathbb{V}(f)}, \quad (11)$$

where $\mathbb{V}(\cdot)$ and $\mathbb{E}[\cdot]$ denote the variance and expectation operators and θ_{-i} is the vector θ without θ_i . The total-effect SI on f includes both the main and higher order effects of θ_i and is

$$\mathcal{T}_i(f) = \frac{\mathbb{E}_{\theta_{-i}}[\mathbb{V}_{\theta_i}(f|\theta_{-i})]}{\mathbb{V}(f)} = 1 - \frac{\mathbb{V}_{\theta_{-i}}(\mathbb{E}_{\theta_i}[f|\theta_{-i}])}{\mathbb{V}(f)}. \quad (12)$$

2.4.2. Time-varying Sobol' indices

The following formulations attempt to account for changes in parameter influence over time.

Pointwise-in-time Sobol' indices (PTSIs): Consider a model f with time-varying output $y(t)$ on the interval $[0, T]$ for $T > 0$, i.e., $y(t) = f(t; \theta)$ for $t \in [0, T]$. The main effect PTISI of f corresponding to θ_i at time t for $t \in [0, T]$ is

$$\mathcal{S}_i(f; t) = \frac{\mathbb{V}_{\theta_i}(\mathbb{E}_{\theta_{-i}}[f(t; \cdot)|\theta_i])}{\mathbb{V}(f(t; \cdot))} \quad (13)$$

and the total effect PTISI at time t is

$$\mathcal{T}_i(f; t) = \frac{\mathbb{E}_{\theta_{-i}}[\mathbb{V}_{\theta_i}(f(t; \cdot)|\theta_{-i})]}{\mathbb{V}(f(t; \cdot))}. \quad (14)$$

Generalized Sobol' indices (GSIs): The PTSIs ignore the variance history of the signal whereas GSIs take it into account by integrating the numerators and denominators of equations (13) and (14) [1]. The main effect GSI over the interval $[0, t]$ for $t \in [0, T]$ is

$$\mathcal{S}_i(f; [0, t]) = \frac{\int_0^t \mathbb{V}_{\theta_i}(\mathbb{E}_{\theta_{-i}}[f(\tau; \cdot)|\theta_i]) d\tau}{\int_0^t \mathbb{V}(f(\tau; \cdot)) d\tau}. \quad (15)$$

Similarly, the total effect GSI of θ_i is

$$\mathcal{T}_i(f; [0, t]) = \frac{\int_0^t \mathbb{E}_{\theta_{-i}}[\mathbb{V}_{\theta_i}(f(\tau; \cdot)|\theta_{-i})] d\tau}{\int_0^t \mathbb{V}(f(\tau; \cdot)) d\tau}. \quad (16)$$

Limited-memory Sobol' indices (LMSIs): By integrating over $[0, t]$, GSIs compute the parameter influence up to time t , which can average the signal and miss parameter contributions during fast, transient disturbances. Hence, we propose a new technique, *limited-memory* Sobol' indices, to analyze parameter influence as the QoI responds to these disturbances. To do so, we introduce a moving integration window of width Δ . Thus, we have the interval $[t - \Delta, t]$ for $t \in [\Delta, T]$. The window shape and magnitude of Δ is problem-dependent. For $t \in [\Delta, T]$, the main effect LMSI of θ_i is

$$\mathcal{S}_i(f; [t - \Delta, t]) = \frac{\int_{t-\Delta}^t \mathbb{V}_{\theta_i}(\mathbb{E}_{\theta_{-i}}[f(\tau; \cdot)|\theta_i]) w(\tau) d\tau}{\int_{t-\Delta}^t \mathbb{V}(f(\tau; \cdot)) w(\tau) d\tau}, \quad (17)$$

where $w(t)$ is the weight determined by the window of choice. Figure 4 gives different options for $w(t)$, which are discussed in detail in Section 4.3. Similarly, the total effect LMSI is

$$\mathcal{T}_i(f; [t - \Delta, t]) = \frac{\int_{t-\Delta}^t \mathbb{E}_{\theta_{-i}}[\mathbb{V}_{\theta_i}(f(\tau; \cdot)|\theta_{-i})] w(\tau) d\tau}{\int_{t-\Delta}^t \mathbb{V}(f(\tau; \cdot)) w(\tau) d\tau}. \quad (18)$$

There are many factors in choosing the appropriate window type, shape, and width. We let the physiology guide our window selection. Since the blood pressure and the change in blood pressure affect the baroreflex modulation of heart rate, recent time points contribute to the current heart rate and future points do not. To accommodate these features, we chose to use a trailing half-Hanning integration window (Figure 4b) for $\Delta = 15$ s to coincide with the typical length of the VM as

$$w(t) = 0.5(1 - \cos(\pi t/T)). \quad (19)$$

2.5. GSA computation

In our numerical experiments, we use Monte Carlo integration to estimate the SIs of all model parameters ($p = 23$) except the VM start and end times, t_s and t_e , which are extracted from data. Specifically, the SIs are calculated using the procedure outlined in Saltelli et al. [29] (page 262, Table 2) that computes the expectations and variances. To test for convergence, we computed $10^3(p + 2) = 25,000$, $10^4(p + 2) = 250,000$, and $10^5(p + 2) = 2,500,000$ function evaluations, which produced similar results [10, 17]. For the reduced models, we use 25,000 evaluations. To approximate the integrals in equations (15)-(18), we used the trapezoid quadrature scheme.

We compare the performance of each of the four methods discussed in Section 2.4. The scalar SIs are calculated with respect to the Euclidean norm of the residual \mathbf{r} (equation (2)), that

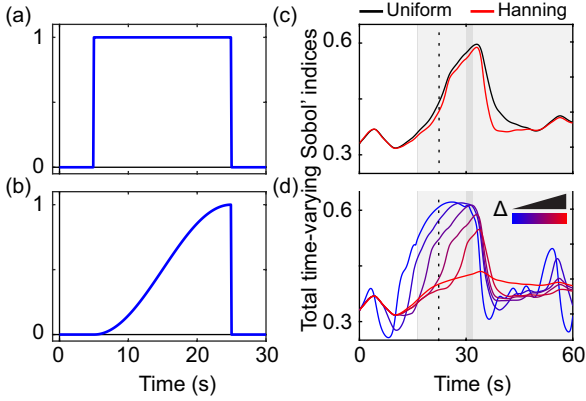


Figure 4: Moving integration window, Δ , for the limited-memory Sobol' indices using parameter H_s as an example. Valsalva maneuver (VM) phases are represented as alternating gray (I and III) and light gray (II and IV) boxes. Phase II is divided into early and late stages (vertical dotted black line). (a) Uniform moving window. (b) Half-Hanning moving window. (c) Comparison of uniform (black) versus Hanning (red) windows of width $\Delta = 15$ s. The Hanning window shows a steeper decline in parameter influence in phase IV. (d) Comparison of varying window lengths for increasing $\Delta = [5, 10, 15, 20]$ s. Pointwise-in-time Sobol' indices (blue) and generalized Sobol' indices (red) are also plotted.

is, $\mathcal{S}_i(\|\mathbf{r}\|_2)$ and $\mathcal{J}_i(\|\mathbf{r}\|_2)$ for \mathbf{r} . Using $\|\mathbf{r}\|_2$ as the scalar model output gives a indication of the average sensitivity of \mathbf{r} to the parameters at steady-state. For the time-varying \mathbf{r} , we simultaneously compute the PTSIs, GSIs, and LMSIs.

2.6. Sensitivity ranking

To identify noninfluential parameters, we rank $\mathcal{J}_i(\|\mathbf{r}\|_2)$ and group them into most, moderately, and least influential. For moderately influential, $\eta_1 = 10^{-1}$ is assigned based on the clear separation in parameter influence (Figure 5). For least influential, $\eta_2 = 10^{-3}$ is assigned in accordance with the LSA from our previous work [26]. The scalar SI groups motivated the grouping used for the PTSIs, GSIs, and LMSIs. We define a parameter θ_i as *noninfluential* over the time series if

$$\mathcal{J}_i(\mathbf{r}; \cdot) < \eta_2 \quad (20)$$

for the entire interval.

2.7. Model reduction

Using the sensitivity ranking, we develop steps for a model reduction methodology informed by the LMSIs. The steps are:

1. Compute the LMSIs for all parameters to be considered.
2. Determine if each $\mathcal{J}_i(f; [t - \Delta, t])$ for $t \in [\Delta, T]$ satisfies equation (20) and make a set of noninfluential parameters, θ_{NI} .
3. Analyze the parameters in θ_{NI} and determine if it is possible to remove the equations associated with each parameter. Choose parameter θ_k that has the least influence. Remove the components of the model associated with that parameter and restructure the model. Some changes to the model equations must occur simultaneously, which we will exemplify in the next section. Note that this step is

problem-specific and inherently changes the mathematical structure of the model. There may be instances where removing model components could be detrimental. Also, there may be instances where there are multiple options available, creating branches of models. Then, analyze the parameters in θ_{NI} of each branch separately.

4. Recalibrate parameters to obtain new parameter vector θ^* for newly generated model f^* . f^* joins the set \mathcal{M} .
5. Repeat steps 1-4 on f^* . Iterate until the equations associated with the noninfluential parameters in θ_{NI} are not algebraically removable. Fix all remaining parameters in θ_{NI} at their nominal values.

This process generates a set of models $\mathcal{M} = \{m_0, m_1, \dots, m_M\}$ for m_0 the original model and m_i the reduced models for $i = 1, \dots, M$.

2.8. Model selection

To compare model performance between the original and reduced models, we compute the AICc and BIC indices, statistical measures that balance the models' fit to the data (goodness of fit) and the model complexity (the number of estimated parameters) [25]. The AICc index, derived from a frequentist perspective, overestimates the model fit to the data, whereas the BIC index, derived from a Bayesian perspective, underestimates it. These indices are commonly calculated for model selection and, if in agreement, provide confidence that the model selected balances over- and underfitting [4]. We assume that the residual errors are independent and identically distributed with mean zero and finite variance. By predicting the maximum likelihood estimate, or equivalently minimizing the least squares error J (equation (C.4)), we compute

$$\text{AICc} = N \log \left(\frac{J}{N} \right) + 2(\hat{p} + 2) \left(\frac{N}{N - (\hat{p} + 2) - 1} \right) \quad \text{and} \quad (21)$$

$$\text{BIC} = N \log \left(\frac{J}{N} \right) + (\hat{p} + 2) \log(N), \quad (22)$$

where N is the number of data points, \hat{p} the dimension of the optimized parameter subset $\hat{\theta}$ [4]. To compare the models, we report the relative index of model m_i from the minimal model, that is,

$$\text{AICc}_{ri} = e^{(\text{AICc}_m - \text{AICc}_i)/2} \quad \text{and} \quad \text{BIC}_{ri} = e^{(\text{BIC}_m - \text{BIC}_i)/2}, \quad (23)$$

where AICc_m and BIC_m are the minimum AICc and BIC values, and AICc_i and BIC_i are the corresponding values for model m_i .

Though this statistical technique is useful when determining the goodness of fit to data, there are predicted model outputs (e.g., T_{pb} and T_s) of clinical importance that cannot be measured without costly and invasive procedures. Therefore, we must also assess the model performance qualitatively. To do so, we compare the reduced models to m_0 , assuming that m_0 produces the true signal. We employ the metric

$$Q = |\max(T_s^{m_0}(t)) - \max(T_s^{m_i}(t))|, \quad (24)$$

where $T_s^{m_0}(t)$ is the baroreflex sympathetic tone $T_s(t)$ from m_0 and $T_s^{m_i}(t)$ is $T_s(t)$ from the reduced model m_i .

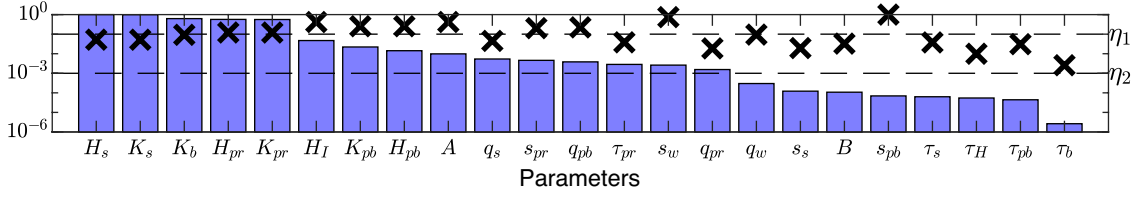


Figure 5: Log-scale relative scalar sensitivity analysis ranking with respect to $\|\mathbf{r}\|_2$. Influence thresholds $\eta_1 = 10^{-1}$ and $\eta_2 = 10^{-3}$ are indicated (horizontal dashed lines). Local analysis results (x's) reproduced from [26] are scaled from zero to one by the maximum sensitivity value. Global analysis results (bars) are computed using the scalar total effect Sobol' indices ($\mathcal{J}_i(\|\mathbf{r}\|_2)$, equation (12)) and scaled by the maximum sensitivity value for comparison with the local results.

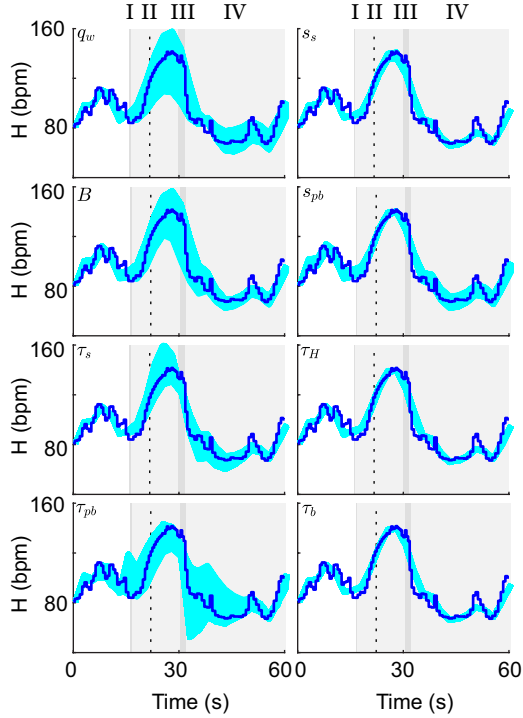


Figure 6: Noninfluential parameters determined by the total effect scalar Sobol' indices in Figure 5. The model was evaluated at 10 equidistant parameter values within the physiological range of each parameter given in Table 1 (cyan) plotted with the heart rate data (blue). The VM phases are represented as alternating gray (I and III) and light gray (II and IV) boxes. Phase II is divided into early and late parts (vertical dotted black line).

3. Results

This section discusses the results regarding the scalar SIs (Figure 5) and the time-varying PTSIs, GSIs, and LMSIs (Figure 7). The latter are computed using a moving integration window of width Δ and several window widths are compared (Figure 4d). For each analysis, the parameters are divided into three influence groups: most ($> \eta_1$), moderately (between η_1 and η_2), and least ($< \eta_2$) influential. Using the LMSIs, we inform a model reduction protocol. Lastly, we select the best model by computing the AIC_c and BIC_r (equation (23)) values in Table 5 and by examining the predicted neural tones T_{pb} and T_s to give physiological predictions (Figure 8).

3.1. Scalar Sobol' indices

The total effect scalar SIs are calculated with respect to $\|\mathbf{r}\|_2$, that is, $\mathcal{J}_i(\|\mathbf{r}\|_2)$ and plotted with LSA results reproduced from [26] (Figure 5). The five most influential parameters, $\{H_s, K_s, K_b, H_{pr}, K_{pr}\}$, are associated with RSA and T_s and affect H during and after the VM. In comparison, the LSA determined that the parameters s_{pb}, s_w, A , and H_I were the most influential. The subset of least influential parameters is

$$\theta_{NI}^S = \{q_w, s_s, B, s_{pb}, \tau_s, \tau_H, \tau_{pb}, \tau_b\}, \quad (25)$$

where the superscript S denotes scalar SIs. Figure 6 displays H when varying each parameter at 10 equidistant points between their upper and lower bounds (given in Table 1) and all other parameters are held fixed. Parameters s_s, s_{pb}, τ_H , and τ_b have the least effect visually on the model output. The small effect of changing s_s and s_{pb} is most likely due to their narrow distributions. In [26], these parameters are calculated *a priori* and do not vary much among the subjects. Parameters τ_H and τ_b have the least effect on the residual for both analyses.

3.2. Pointwise-in-time Sobol' indices

Figure 7 shows results for the most (Figure 7a), moderately (Figure 7d), and least (Figure 7g) influential parameters for the PTSIs, which display rapid fluctuations. The most influential parameters, H_s, K_s, K_b, H_{pr} , and K_{pr} (Figure 7a), correspond to the scalar SIs. Our results show that the index for K_b does not change significantly during the time interval, which is expected since the baroreceptors are always active. Parameters K_s and H_s are most influential due sympathetic activation after the breath hold. Finally, H_{pr} and K_{pr} decrease in influence below η_1 after the breath hold due to parasympathetic withdrawal.

Parameters s_s and s_{pb} remain below η_2 for all time. Though all other time-scales rise above η_2 , τ_b surprisingly also remains below η_2 . These insensitive parameters are prime candidates for removal. Overall, the PTSIs designate almost all parameters as at least moderately influential, which agree with the LSA results. However, these results do not provide much additional information that is not already given in the scalar SIs.

3.3. Generalized Sobol' indices

As shown in Figures 7b, e, and h, the GSIs smooth the signals, placing much emphasis on the time-dependence and averaging the signal over extended periods of baseline activity. They miss potential transient changes in parameter influence on the model

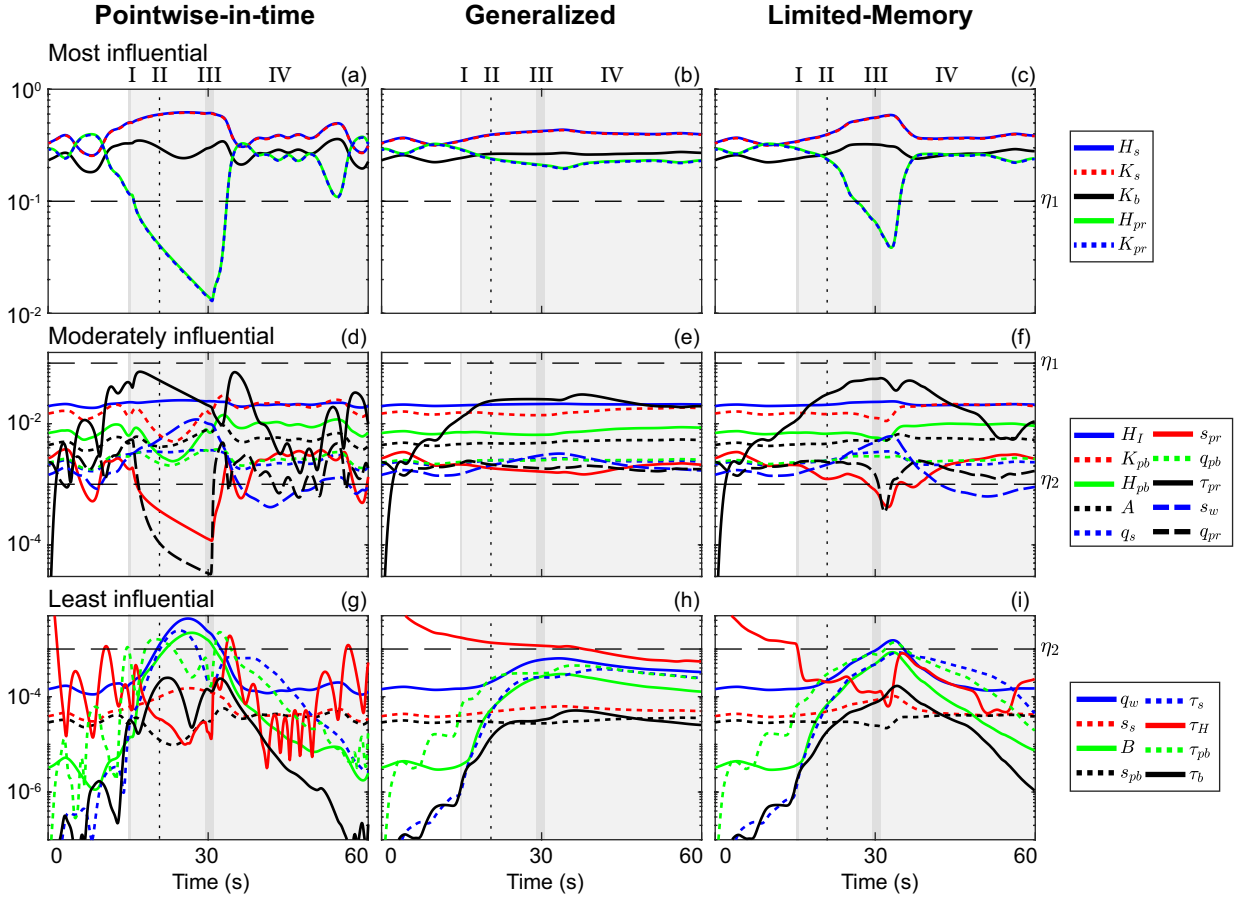


Figure 7: Time-varying total effect Sobol' indices (SIs) for the most (top row), moderately (middle row), and least (bottom row) influential parameters determined by the scalar SIs in Figure 5 for the pointwise-in-time (a, d, g), generalized (b, e, h), and limited-memory (c, f, i) SIs. Thresholds $\eta_1 = 10^{-1}$ and $\eta_2 = 10^{-3}$ are indicated with horizontal dashed black lines. The VM phases are represented as alternating gray (I and III) and light gray (II and IV) boxes. Phase II is divided into early and late parts (vertical dotted black line). Results are plotted on a logarithmic scale for the y-axis.

output. PTSIs and GSIs provide extremes for analyzing time-varying signals as shown in Figure 4d (PTSI in blue and GSI in red). These results suggest that there is a need for a method that incorporates both the transient nature of the PTSIs and the smoothing capabilities of the GSIs.

The GSI for τ_H (Figure 7h) fluctuates significantly. τ_H is moderately influential at the beginning but decreases in influence after the onset of the VM. Hence, τ_H may play a role in establishing steady-state behavior from the initial conditions and then decrease in influence once steady-state is achieved. As shown in Figure 7h, the least influential subset of parameters determined by the GSIs is

$$\theta_{NI}^G = \{q_w, s_s, B, s_{pb}, \tau_s, \tau_{pb}, \tau_b\}, \quad (26)$$

where the superscript G denotes generalized SIs.

3.4. Limited-memory Sobol' indices

For the LMSIs, it is important to choose a window that is short enough so as to retain important features but long enough to be easily interpretable. Since the VM typically lasts 15 s, we compare the output from several window widths for $\Delta = 5, 10, 15$, and 20 s (Figure 4d). For smaller values of Δ , the LMSI tends

toward the PTSI whereas for larger values of Δ , the LMSI tends toward the GSI. To remain consistent with the VM itself, we chose a window of 15 s.

Fluctuations in parameter influence correspond to different control mechanisms that activate and deactivate during the VM. The LMSIs remain relatively constant before the VM (Figures 7c, f, and i). We observe increases in influence of parameters associated with T_s during the VM that decrease afterward. This behavior coincides with the activation and deactivation of T_s during the VM. Note that q_w and τ_{pb} become moderately influential during the VM while the subset

$$\theta_{NI}^{LM} = \{s_s, B, s_{pb}, \tau_s, \tau_b\}, \quad (27)$$

where superscript LM denotes limited-memory, remains below η_2 . τ_b has consistently been the least influential throughout all analyses. Surprisingly, B and τ_s also remain below η_2 for all t .

In summary, the scalar SIs and LSA provide clear parameter influence rankings. However, the time-varying techniques elucidate *when* a parameter becomes influential. Our results show that the GSIs have a clear benefit over the PTSIs, incorporating the signal history, but miss the effects of transient disturbances. We conclude that the LMSIs illustrate parameter influence traces that correspond to the modeled physiological

Table 3: Noninfluential (NI) parameters.

Parameters	θ_{NI}^S (25)	θ_{NI}^G (26)	θ_{NI}^{LM} (27)
q_w	✓	✓	
s_s	✓	✓	✓
B	✓	✓	✓
s_{pb}	✓	✓	✓
τ_s	✓	✓	✓
τ_H	✓		
τ_{pb}	✓	✓	
τ_b	✓	✓	✓

S - scalar. G - generalized. LM - limited memory.

Table 4: Estimated parameter values.

Parameters	m_0	m_1	m_2	m_3	m_4
B	0.43	0.43	0.58	0 [†]	1 [†]
τ_{pb}	4.27	4.27	4.05	3.85	4.62
τ_{pr}	2.71	2.71	2.61	2.68	2.58
H_{pb}	0.43	0.43	0.43	0.42	0.43
H_{pr}	0.48	0.48	0.46	0.50	0.39
H_s	0.28	0.28	0.32	0.20	0.47

[†] held constant and excluded from estimation.

phenomena. Table 3 summarizes the subsets of noninfluential parameters from the scalar SIs (equation (25)), GSIs (equation (26)), and LMSIs (equation (27)). The PTSIs were not included as their results were inconclusive. The LMSIs determined the smallest subset with 5 noninfluential parameters considered for removal.

3.5. Model reduction

We “remove” a parameter from consideration by fixing it at its nominal value or analytically excising equations associated with it. In Section 3.5.1, we consider the parameters in equation (27) to fix at their nominal values. In Sections 3.5.2 and 3.5.3, we remove equations associated with noninfluential parameters and develop a suite of models upon which we can perform statistics.

3.5.1. Fixed parameters

Parameters s_{pb} and s_s (equations (A.13) and (A.14)) are computed *a priori* assuming 80% of the baseline heart rate is controlled by T_{pb} and 20% by T_s [26]. The coefficient of variation (SD/mean) for both is $\sim 0.1\%$, which implies a very narrow dispersion. In [27], we show that τ_s (equation (A.4)) is nonlinearly related to D_s , which can lead to instability. Therefore, we restricted the bounds of τ_s to $\pm 50\%$ of the nominal value (Table 1) to ensure model stability. After fixing these parameters at their nominal values, we recalculated the LMSIs with 25,000 samples, which produced similar results to Figure 7i with τ_b and B still in θ_{NI}^{LM} (results not shown). This process produces the reduced model, m_1 , for which s_{pb} , s_s , and τ_s are constant. Table 4 lists parameters for m_0 and m_1 . Note that both models have the same estimated parameters. Therefore, from here on, we compare further reduced models to m_1 . τ_b and B are removed and the equations impacted by these parameters are modified as described in the following sections.

3.5.2. Removing τ_b

Since τ_b (equations (A.1) and (A.2)) can be small with negligible impact, we rearrange equation (A.1) as

$$\tau_b \frac{d\varepsilon_{bc}(t)}{dt} + \varepsilon_{bc}(t) = K_b G_{bc}(t). \quad (28)$$

By letting $\tau_b = 0$, equations (A.1) and (A.2) become $\varepsilon_{bc}^*(t) = K_b G_{bc}(t)$ and $\varepsilon_{ba}^*(t) = K_b G_{ba}(t)$, respectively. From here on, an asterisk denotes the reduced system. Note that the dimension of the state space has reduced by two. Substituting ε_{bc}^* and ε_{ba}^* into equation (8) gives

$$\begin{aligned} n(t) &= B(G_{bc}(t) - \varepsilon_{bc}^*(t)) + (1 - B)(G_{ba}(t) - \varepsilon_{ba}^*(t)) \\ &= (1 - K_b)n^*(t), \end{aligned} \quad (29)$$

where

$$n^*(t) = BG_{bc}(t) + (1 - B)G_{ba}(t). \quad (30)$$

By substituting equation (29) into equation (A.13), we obtain

$$G_{pb}^*(t) = \frac{1}{1 + e^{-q_{pb}(n(t) - s_{pb})}} = \frac{1}{1 + e^{-q_{pb}^*(n^*(t) - s_{pb}^*)}}, \quad (31)$$

and define new parameter values

$$q_{pb}^* = q_{pb}(1 - K_b) \quad \text{and} \quad s_{pb}^* = \frac{s_{pb}}{1 - K_b}. \quad (32)$$

$G_s(t)$ also reduces to $G_s^*(t)$ with new parameters q_s^* and s_s^* (equation (A.21)). Note that K_b is used to calculate q_{pb}^* , s_{pb}^* , q_s^* , and s_s^* , and hence, the dimension of Ω_p is reduced by one.

The reduced system consists of 4 states and 23 parameters

$$\frac{d\mathbf{x}^*(t)}{dt} = f^*(t, \mathbf{x}^*(t), \mathbf{x}^*(t - D_s); \theta^*), \quad (33)$$

where $\mathbf{x}^*(t) = [T_{pb}(t), T_{pr}(t), T_s(t), H(t)]^T \in \mathbb{R}^4$ and

$$\begin{aligned} \theta^* &= [A, B, K_{pb}, K_{pr}, K_s, \tau_{pb}, \tau_{pr}, \tau_s, \tau_H, q_w, q_{pb}^*, q_{pr}, q_s^*, \\ & s_w, s_{pb}^*, s_{pr}, s_s^*, H_I, H_{pb}, H_{pr}, H_s, t_s, t_e]^T \in \mathbb{R}^{23}. \end{aligned} \quad (34)$$

Note that θ^* does not contain K_b . The full set of equations of f^* are in Appendix A. We refer to this reduced model as m_2 .

We perform subset selection using the structured correlation analysis described in Appendix C to determine a subset of parameters to optimize for m_2 and obtain

$$\hat{\theta}^{m_2} = [B, \tau_{pb}, \tau_{pr}, H_{pb}, H_{pr}, H_s]^T. \quad (35)$$

Table 4 lists the optimized parameters for m_2 . We perform GSA on m_2 , holding s_{pb} , s_s , and τ_s fixed, and observe that B is the only parameter below η_2 for all time t (results not shown).

3.5.3. Removing B

The necessity of delineating the aortic and carotid regions has been explored in two previous studies [15, 26] and, surprisingly, B is flagged for removal. Note that when $B = 0$ in equation (30), the aortic strain solely influences the efferent response,

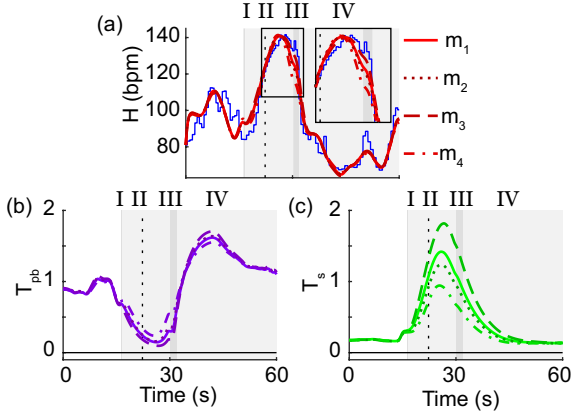


Figure 8: Plots of the reduced model 1 (m_1 , solid), 2 (m_2 , dotted), 3 (m_3 , dashed), and 4 (m_4 , dash-dotted). The original model m_0 has been omitted since it has the same estimated parameters as m_1 (Table 4). The Valsalva maneuver (VM) phases are represented as alternating gray (I and III) and light gray (II and IV) boxes. Phase II is divided into early and late stages (vertical dotted black line). (a) Model fits (red) to heart rate data (blue). Insert shows a zoom in late phase II and phase III. (b) Model predictions of baroreflex-mediated parasympathetic (T_{pb} , purple) for the full and reduced models. (c) Model predictions of baroreflex-mediated sympathetic (T_s , green) for the original and reduced models.

and when $B = 1$, the carotid. It is unknown how these signals are integrated in the medulla and not clear whether it is sufficient to model only one of them. We observe that the LMSI of B is small initially, increases as the VM progresses, and decreases after the breath hold (Figure 7i). This produces two models branching from m_2 : m_3 where $B = 0$ and $n_2^*(t) = G_{ba}(t)$ and m_4 where $B = 1$ and $n_3^*(t) = G_{bc}(t)$. These are systems of ODEs and DDEs with 4 states and 22 parameters of the form in equation (33). Appendix A contains more details for the construction of m_3 and m_4 . Table 4 lists the estimated parameters for m_3 and m_4 . We perform GSA on each, which results in all parameters above η_2 at some time point (results not shown). Hence, there are no parameters remaining in the noninfluential subset.

In summary, the model reduction methodology has produced 5 possible models (Table 4): m_0 , the original model; m_1 , the original model with s_{pb} , s_s , and τ_s fixed; m_2 reduced model removing τ_b ; m_3 reduced model removing τ_b and setting $B = 0$; and m_4 reduced model removing τ_b and setting $B = 1$. Figure 8 plots the model fits to the data as well as their respective neural tones.

3.6. Model selection

To determine which model best fits the data, we perform model selection quantitatively by computing $AICc_r$ and BIC_r (equation (23)) and qualitatively by comparing T_{pb} and T_s of the reduced models to m_0 . The latter is important since our goal is not only to fit the data but also to predict the neural tones that cannot be measured *in vivo*.

3.6.1. Goodness of fit analysis

Table 5 shows that m_2 has the greatest $AICc_r$ and BIC_r values. This is surprising since m_2 estimates more model parameters

Table 5: Statistical analysis for model selection.

Model	Cost J (10^{-3}) (C.4)	Pars p	Quantitative		Qualitative
			$AICc_r$ (23)	BIC_r (23)	Q (24)
m_0	4.64	6	0.83	0.83	
m_1	4.64	6	0.83	0.83	0
m_2	4.63	6	1	1	0.17
m_3	4.97	5	$2.5e-4$	$3.6e-4$	0.41
m_4	4.97	5	$2.5e-5$	$3.6e-5$	0.48

Pars - number of parameters. $AICc_r$ - Akaike Information Criterion with correction. BIC_r - Bayesian Information Criterion.

than both m_3 and m_4 . This analysis suggests that modeling both the regions is necessary to predict heart rate.

3.6.2. Qualitative assessment

Figure 8 shows H , T_{pb} , and T_s for all of the models considered: m_1 (solid curve), m_2 (dotted curve), m_3 (dashed curve) and m_4 (dash-dotted curve). The model fits to heart rate data (Figure 8a) are all similar, which is expected. The least squares costs of the fits are of the same magnitude (Table 5). Interestingly, m_3 is the only model that is able to fit phase III of the data (Figure 8a insert), suggesting from a qualitative standpoint that m_3 captures the most features of the heart rate data. Figure 8b displays the predicted T_{pb} trace for the models, which are all similar. Figure 8c shows that T_s , exhibits the greatest deviation from m_0 . Thus, we use T_s to compare the reduced models to m_0 via the Q value (equation (24)). Table 5 compiles these metrics and m_2 has the lowest Q value, suggesting that both regions must be included. Hence, we conclude that m_2 is the best model for the biological questions investigated here since the $AICc_r$ and BIC_r values are the greatest while the qualitative metric Q was the lowest.

4. Discussion

This study performs model reduction and selection using GSA on a cardiovascular model predicting heart rate (H) in response to the VM. Computation for the scalar SIs [29] was done with respect to $\|\mathbf{r}\|_2$ while the time-varying PTSIs [2], GSIs [1], and LMSIs are with respect to \mathbf{r} . A novel component of this study is the introduction of the LMSIs using a moving integration window Δ motivated by the transient VM. The scalar SIs determined a ranking of parameter influence, from which we created three groups: most, moderately, and least influential. Additionally, the LMSIs informed a model reduction protocol that generated five models: m_0 , m_1 , m_2 , m_3 , and m_4 . We analyzed the performance of these models quantitatively, calculating the $AICc_r$ and BIC_r (equation (23)) values, and qualitatively, comparing the model predicted signals to the original model m_0 , Q (equation (24)). From this analysis, m_2 is the best model, suggesting that modeling both the aortic and carotid baroreceptor regions are necessary to predict heart rate and neural tones.

4.1. Local versus global sensitivity analysis

This study focused on using GSA to analyze the influence of the parameters on the model output. These methods are computationally expensive, whereas LSA methods may suffice. In

[26], we performed LSA on the neural model, reproduced in Figure 5. LSA is useful in its (i) relative ease in computation and (ii) ability to calculate time-varying sensitivities. In steady-state with nominal parameters close to their optimal value, LSA is useful in ranking parameter influence [6, 20, 23]. The results from the LSA are similar to the ranking of the scalar SIs. Since every parameter in the LSA was above $\eta_2 = 10^{-3}$, every parameter is influential. However, this is a snapshot of the model sensitivity at one instance in Ω_p . The benefit of GSA is that it explores the entirety of Ω_p and incorporates parameter interactions. Though there are some differences, the parameter rankings for both the LSA and scalar SIs are similar overall, which could be due to the *a priori* calculation of nominal parameter values. Others have also found agreement in the calculation of the local and global parameter influences [17].

4.2. Time-varying GSA

Though there are other methods that explore Ω_p [22, 34], we used SIs due to their broad applications. Here, we introduce LMSIs that provide a more informative ranking than scalar SIs during a transient disturbance from baseline. They smooth the oscillatory PTSIs and incorporate the variance history preserved by the GSIs. The LMSIs retain some modulation, providing distinct changes in parameter influence rankings before, during, and after the VM. Lastly, they can be used for virtually any modeling effort analyzing parameter influence over time.

Not every problem requires time-varying GSA, which depends on the questions asked and the QoI. Scalar SIs are appropriate if the QoI is a scalar, in steady-state, at a particular time point, or periodic. If the objective is to understand parameter influence during state transition, time-varying GSA may provide rich information. One such study is that of Calvo et al. [5], which calculated SIs for the parameters of a cardiovascular model studying head-up tilt at rest and during the tilt. The state transition as the tilt occurs is of great clinical interest, and hence, this study can benefit from using LMSIs to measure changes in parameter influence. Another is the study by Sumner et al. [36] that claims to analyze time-dependent parameter influence with SIs. However, the QoI for this model is a state evaluated at time point $t = 60$, which is a scalar value. If other time points are of interest, either GSIs or LMSIs can be used to quantify the parameter influence over time.

4.3. Integration window

Moving windows have been used in signal processing for decades and recently in graphical sensitivity analysis [12, 35], typically smoothing signals. There are several considerations when choosing an appropriate Δ for analysis of a biological problem: shape, type, and width. Shape refers to the functional form providing the weights for the window. There are many potential window shapes, but uniform (Figure 4a) and Hanning (Figure 4b) windows are common. A uniform window applies equal weight to each t_j whereas a half-Hanning places more emphasis on the most recent time points. Figure 4c compares the traces from both a uniform (black) and a Hanning (red) shape, though the differences are negligible. For the physiological application examined here, the only reasonable window type is a

trailing window. Width refers to the time interval over which the window applies. We chose $\Delta = 15$ s to correspond with the VM. We strongly suggest allowing the features of the system studied to dictate choice of window.

4.4. Model reduction

Due to the overall model complexity, understanding the biological implications of the results and parameter interactions can be difficult. Therefore, model reduction can simplify these interactions and still retain its predictive power. Many model reduction techniques exist from engineering and control theory [3], aiming to reduce large numbers of state variables with many nonlinearities by attempting to mitigate the extent that the input parameters affect the output. Our method using GSA to inform an analytical model reduction uses this idea to make appropriate choices for the exclusion of certain model components, unlike methods that solely approximate input-output relationships without considering other predicted model quantities [31]. To our knowledge, there are no previous studies that inform a model reduction based on time-varying GSA methods for physiological models. For biological systems with scalar QoIs, there has been a methodology proposed for model reduction via GSA by Marino et al. [19]; however, a statistical analysis of a group of reduced models was not conducted. Furthermore, we propose our GSA-informed model reduction methodology as an alternative approach to the balanced truncation method [31].

Though we acknowledge that SIs may be impractical for large ODE systems (e.g. pharmacokinetics models), we suggest a multi-level approach. One can use GSA measures that are simpler to compute but possibly less informative first to identify a set of unimportant parameters and then perform a more comprehensive analysis on the remaining parameters [11].

4.5. Model selection

Previous studies have modeled baroreceptor stimulation of only the carotid region [16, 18], though to our knowledge there are no studies solely modeling the aortic baroreceptors. To our knowledge, no previous studies have performed a model selection protocol for cardiovascular models in response to the VM. To consider the effect of reducing m_0 on the predicted quantities, we combine quantitative and qualitative approaches to select whether delineating between carotid and aortic regions is necessary, and, if not, which pathway should be modeled. We perform our analysis on our set of models $\mathcal{M} = \{m_0, m_1, m_2, m_3, m_4\}$, and results show that m_2 has the greatest AIC_c and BIC_r values and the lowest Q value. Ultimately, we conclude that m_2 is the best model both to fit the heart data and predict the neural tones, and therefore, both regions are necessary to model the VM, agreeing with previous studies [15, 26].

4.6. Limitations

The GSA method of choice is dependent on the model formulation and the QoI. GSA may not be feasible for computationally intensive models. GSA results will differ based on the choice of QoI. For our GSA, SIs assume that the model parameters are

statistically independent, which may not be reasonable. Furthermore, analytical model reduction may be impractical for large systems. In this case, setting noninfluential parameters to their nominal values may be more reasonable. Lastly, using $AICc_r$ and BIC_r values is dependent on available data. If a different heart data set had been used, the outcome of the model selection protocol could be different. However, we conducted this analysis on three representative subjects and achieved similar results (not shown).

5. Conclusions

In this study, we introduced a model reduction and selection methodology informed by global sensitivity analysis on a model predicting heart rate and autonomic function in response to the Valsalva maneuver. We developed the novel limited-memory Sobol' indices that account for both the variance history and transient dynamics. Furthermore, with extensive numerical experiments, we simplified the model while retaining important physiological characteristics. We conclude that modeling both the aortic and carotid regions is necessary to achieve the appropriate dynamics of the Valsalva maneuver.

6. Acknowledgments

We would like to thank Dr. Pierre Gremaud for his help developing and analyzing the limited-memory Sobol' indices.

7. Funding

This study was supported in part by the National Science Foundation under awards NSF/DMS 1246991 and NSF/DMS 1557761 and by the National Institute of Health HL139813.

Appendix A. Model equations

This appendix lists the equations for the original model, m_0 , and the reduced models, m_1 , m_2 , m_3 , and m_4 , given in Section 2.

Original model. m_0 (Section 2.3) has 6 states and 25 parameters of the form in equation (3). The system f [26] consists of the following set of equations:

$$\frac{d\varepsilon_{bc}(t)}{dt} = \frac{1}{\tau_b}(-\varepsilon_{bc}(t) + K_b G_{bc}(t)), \quad (\text{A.1})$$

$$\frac{d\varepsilon_{ba}(t)}{dt} = \frac{1}{\tau_b}(-\varepsilon_{ba}(t) + K_b G_{ba}(t)), \quad (\text{A.2})$$

$$\frac{dT_{pb}(t)}{dt} = \frac{1}{\tau_{pb}}(-T_{pb}(t) + K_{pb} G_{pb}(t)), \quad (\text{A.3})$$

$$\frac{dT_s(t)}{dt} = \frac{1}{\tau_s}(-T_s(t - D_s) + K_s G_s(t)), \quad (\text{A.4})$$

$$\frac{dT_{pr}(t)}{dt} = \frac{1}{\tau_{pr}}(-T_{pr}(t) + K_{pr} G_{pr}(t)), \quad (\text{A.5})$$

$$\frac{dH(t)}{dt} = \frac{1}{\tau_H}(-H(t) + \tilde{H}(t)), \quad (\text{A.6})$$

$$P_t(t) = \begin{cases} \text{ITP}(t) & t_s \leq t \leq t_e \\ \frac{R_M - R_m}{\bar{R}_I - \bar{R}_E} R(t) + (R_m - \bar{R}_E) & \text{otherwise} \end{cases}, \quad (\text{A.7})$$

$$P_c(t) = \text{SBP}(t), \quad (\text{A.8})$$

$$P_a(t) = \text{SBP}(t) - P_t(t), \quad (\text{A.9})$$

$$G_{bc}(t) = 1 - \sqrt{\frac{1 + e^{-q_w(P_c(t) - s_w)}}{A + e^{-q_w(P_c(t) - s_w)}}}, \quad (\text{A.10})$$

$$G_{ba}(t) = 1 - \sqrt{\frac{1 + e^{-q_w(P_a(t) - s_w)}}{A + e^{-q_w(P_a(t) - s_w)}}}, \quad (\text{A.11})$$

$$n(t) = B(G_{bc}(t) - \varepsilon_{bc}(t)) + (1 - B)(G_{ba}(t) - \varepsilon_{ba}(t)), \quad (\text{A.12})$$

$$G_{pb}(t) = \frac{1}{1 + e^{-q_{pb}(n(t) - s_{pb})}}, \quad (\text{A.13})$$

$$G_s(t) = \frac{1}{1 + e^{q_s(n(t) - s_s)}}, \quad (\text{A.14})$$

$$G_{pr}(t) = \frac{1}{1 + e^{-q_{pr}(P_r(t) - s_{pr})}}, \quad (\text{A.15})$$

$$\tilde{H}(t) = H_I(1 - H_{pb}T_{pb}(t) + H_{pr}T_{pr}(t) + H_sT_s(t)). \quad (\text{A.16})$$

Reduced models. The reduced model for m_1 has the same equations as m_0 . m_2 (Section 3.5) has 4 states and 23 parameters and is of the form in equation (33). The system f^* consists of equations (A.5) - (A.11), equation (A.15), and the equations:

$$\frac{dT_{pb}(t)}{dt} = \frac{1}{\tau_{pb}}(-T_{pb}(t) + K_{pb} G_{pb}^*(t)), \quad (\text{A.17})$$

$$\frac{dT_s(t)}{dt} = \frac{1}{\tau_s}(-T_s(t - D_s) + K_s G_s^*(t)), \quad (\text{A.18})$$

$$n^*(t) = B G_{bc}(t) + (1 - B) G_{ba}(t), \quad (\text{A.19})$$

$$G_{pb}^*(t) = \frac{1}{1 + e^{-q_{pb}^*(n^*(t) - s_{pb}^*)}}, \quad (\text{A.20})$$

$$G_s^*(t) = \frac{1}{1 + e^{q_s^*(n^*(t) - s_s^*)}}, \quad (\text{A.21})$$

For reduced model m_3 , $B = 0$, equation (A.19) becomes $n_2^*(t) = G_{ba}(t)$, and (A.8) and (A.10) are eliminated. For m_4 , $B = 1$, equation (A.19) becomes $n_3^*(t) = G_{bc}(t)$, (A.7), (A.9), and (A.11) are eliminated.

Appendix B. Initial conditions

This appendix contains calculations of the initial conditions (ICs) for f in equation (3) computed to ensure the model is in steady-state. The ICs take into account the baseline systolic blood pressure \bar{P} , thoracic pressure \bar{P}_t , and heart rate \bar{H} , that is, $\bar{P}_c = \bar{P}$ and $\bar{P}_a = \bar{P} - \bar{P}_t$. We let $\bar{\cdot}$ denote steady-state. The ICs for ε_{bc} and ε_{ba} (equations (A.1) and (A.2)) are

$$\bar{\varepsilon}_{bc} = K_b \bar{G}_{bc} = K_b \left(1 - \sqrt{\frac{1 + e^{-q_w(\bar{P}_c - s_w)}}{A + e^{-q_w(\bar{P}_c - s_w)}}} \right) \quad \text{and} \quad (\text{B.1})$$

$$\bar{\varepsilon}_{ba} = K_b \bar{G}_{ba} = K_b \left(1 - \sqrt{\frac{1 + e^{-q_w(\bar{P}_a - s_w)}}{A + e^{-q_w(\bar{P}_a - s_w)}}} \right). \quad (\text{B.2})$$

The ICs $\bar{T}_{pb} = 0.8$ and $\bar{T}_s = 0.2$ are based on the assumption that 80% of baroreflex contribution to H is due to the parasympathetic tone and 20% due to sympathetic [26]. The IC for the RSA-mediated parasympathetic tone is

$$\bar{T}_{pr} = K_{pr} \bar{G}_{pr} = \frac{K_{pr}}{1 + e^{-q_{pr}(\bar{P}_t - s_{pr})}}. \quad (\text{B.3})$$

The IC for the model output heart rate is \bar{H} .

Appendix C. Subset selection and parameter estimation

This appendix provides details concerning parameter subset selection and estimation. We determine a subset of parameters $\hat{\theta}$ to optimize using structured correlation analysis [23, 24]. The i^{th} column of a sensitivity matrix (\mathbf{S}) of the model residual \mathbf{r} with respect to the logarithm of the parameters at time t_j is

$$S_{ij} = \frac{\partial \mathbf{r}(t_j)}{\partial \log \theta_i} = \frac{\partial H(t_j; \theta)}{\partial \theta_i} \frac{\theta_i}{H_d(t_j)} \quad (\text{C.1})$$

for H the model output heart rate and H_d the data. Note that this analysis is local. To determine possible pairwise correlations between influential parameters [23], we calculate a correlation matrix \mathbf{c} from a covariance matrix $\mathbf{C} = (\hat{\mathbf{S}}^T \hat{\mathbf{S}})^{-1}$ as

$$c_{ij} = \frac{C_{ij}}{\sqrt{C_{ii} C_{jj}}}, \quad (\text{C.2})$$

where $\hat{\mathbf{S}}$ is a matrix with the columns of \mathbf{S} corresponding to the parameters in $\hat{\theta}$. \mathbf{c} is symmetric with $|c_{ii}| = 1$ and $|c_{ij}| \leq 1$. We assigned a threshold of 0.9 for correlated parameters.

We removed some parameters from consideration *a priori*, such as all q_x and s_x . Optimizing these parameters can force the model to produce results that are not physiological [26]. We also excluded t_s and t_e from consideration as they were determined directly from the data and are naturally very influential.

From these methods, we obtain the identifiable subset for the original model as

$$\hat{\theta} = [B, \tau_{pb}, \tau_{pr}, H_{pb}, H_{pr}, H_s]^T. \quad (\text{C.3})$$

More details can be found in [26]. Given \mathbf{r} (equation 1), we fit H to data by minimizing the least squares cost

$$J(\hat{\theta}) = \mathbf{r}(t)^T \mathbf{r}(t) + \left(\frac{\max_j H_m(t_j; \theta) - \max_j H_d(t_j)}{\max_j H_d(t_j)} \right)^2. \quad (\text{C.4})$$

References

References

- [1] A. Alexanderian, P. A. Gremaud, R. C. Smith. Variance-based sensitivity analysis for time-dependent processes. *Reliab Eng Syst Safe*, 196: 1–17. 2020. DOI: 10.1016/j.res.2019.106722.
- [2] A. Alexanderian, J. Winokur, I. Sraj, A. Srinivasa, M. Iskandarani, W. C. Thacker, O. M. Knio. Global sensitivity analysis in an ocean general circulation model: a sparse spectral projection approach. *Comput Geosci*, 16 (3): 757–778. 2012. DOI: 10.1007/s10596-012-9286-2.
- [3] B. Besselink, U. Tabak, A. Lutowska, N. van de Wouw, H. Nijmeijer, D. J. Rixen, M. E. Hochstenbach, W. H. A. Schilders. A comparison of model reduction techniques from structural dynamics, numerical mathematics, and systems and control. *J Sound Vib*, 332 (19): 4403–4422. 2013. DOI: 10.1016/j.jsv.2013.03.025.
- [4] K. P. Burnham, D. R. Anderson. *Model selection and multimodel inference: a practical information-theoretic approach*. 2nd Edition, Springer-Verlag, New York, 2002. DOI: 10.1007/b97636.
- [5] M. Calvo, V. Le Rolle, D. Romero, N. Behar, P. Gomis, P. Mabo, A. I. Hernandez. Global sensitivity analysis of a cardiovascular model for the study of the autonomic response to head-up tilt testing. in: *Conf Proc IEEE Eng Med Biol Soc*, 5458–5461. 2018. DOI: 10.1109/EMBC.2018.8513536.
- [6] L. M. Ellwein, H. T. Tran, C. Zapata, V. Novak, M. S. Olufsen. Sensitivity analysis and model assessment: mathematical models for arterial blood flow and blood pressure. *Cardiovasc Eng* 8 (2): 94–108. 2008. DOI: 10.1007/s10558-007-9047-3.
- [7] F. Gamboa, A. Janon, T. Klein, A. Lagnoux. Sensitivity analysis for multi-dimensional and functional outputs. *Electron J Stat* 8 (1):575–603. 2014. DOI: 10.1214/14-EJS895
- [8] N. Guglielmi, E. Hairer. Implementing Radau IIA methods for stiff delay differential equations. *Computing* 67 (1): 1–12. 2001. DOI: 10.1007/s006070170013.
- [9] W. F. Hamilton, R. A. Woodbury, H. T. Harper, Jr. Arterial, cerebrospinal and venous pressures in man during cough and strain. *Am J Physiol* 141 (1): 42–50. 1944. DOI: 10.1152/ajplegacy.1944.141.1.42.
- [10] J. L. Hart. *Extensions of global sensitivity analysis: theory, computation, and applications*. Ph.D. thesis, North Carolina State University. 2018.
- [11] J. L. Hart, P. A. Gremaud, T. David. Global sensitivity analysis of high-dimensional neuroscience models: an example of neurovascular coupling. *Bull Math Biol* 81: 1805–1828. 2019. DOI: 10.1007/s11538-019-00578-0.
- [12] B. Iooss, P. Lemaitre. A review on global sensitivity analysis methods. in: *Uncertainty Management in Simulation-Optimization of Complex Systems: Algorithms and Applications*. Research/Computer Science Interfaces Series, Springer, Boston, MA, 59: 101–122. 2015. DOI: 10.1007/978-1-4899-7547-8_5
- [13] F. Kappel, M. Munir. Generalized sensitivity functions for multiple output systems. *J Inverse Ill-Posed Probl* 25 (4): 499–519. 2017. DOI: 10.1515/jiip-2016-0024.
- [14] A. Kipariisides, S. S. Kucherenko, A. Mantalaris, E. N. Pistikopoulos. Global sensitivity analysis challenges in biological systems modeling. *Ind Eng Chem Res* 48 (15): 7168–7180. 2009. DOI: 10.1021/ie900139x.
- [15] S. A. Kosinski, B. E. Carlson, S. L. Hummel, R. D. Brook, D. A. Beard. Computational model-based assessment of baroreflex function from response to Valsalva maneuver. *J Appl Physiol* 125 (6): 1944–1967. 2018. DOI: 10.1152/jappphysiol.00095.2018.
- [16] V. Le Rolle, A. I. Hernandez, P. Y. Richard, G. Carrault. An autonomic nervous system model applied to the analysis of orthostatic tests. *Model Simul Eng* 2008: 1–15. 2008. DOI: 10.1155/2008/427926.
- [17] K. G. Link, M. T. Stobb, J. Di Paola, K. B. Neevees, A. L. Fogelson, S. S. Sindi, K. Leiderman. A local and global sensitivity analysis of a mathematical model of coagulation and platelet deposition under flow. *PLoS One* 13 (7): 1–38. 2018. DOI: 10.1371/journal.pone.0200917.
- [18] K. Lu, J. W. Clark Jr., F. H. Ghorbel, D. L. Ware, A. Bidani. A human cardiopulmonary system model applied to the analysis of the Valsalva maneuver. *Am J Physiol Heart Circ Physiol* 281 (6): H2661–H2679. 2001. DOI: 10.1152/ajpheart.2001.281.6.H2661.
- [19] S. Marino, I. B. Hogue, C. J. Ray, D. E. Kirschner. A methodology for performing global uncertainty and sensitivity analysis in systems biology. *J Theor Biol* 254 (1): 178–196. 2008. DOI: 10.1016/j.jtbi.2008.04.011.

- [20] A. D. Marquis, A. Arnold, C. Dean-Bernhoft, B. E. Carlson, M. S. Olufsen. Practical identifiability and uncertainty quantification of a pulsatile cardiovascular model. *Math Biosci* 304: 9–24. 2018. DOI: 10.1016/j.mbs.2018.07.001.
- [21] M. D. Morris. Factorial sampling plan for preliminary computational experiments. *Technometrics* 33 (2): 161–174. 1991. DOI: 10.2307/1269043.
- [22] C. H. Olsen, J. T. Ottesen, R. C. Smith, M. S. Olufsen. Parameter subset selection techniques for problems in mathematical and biology. *Biol Cybern* 113 (1-2): 121–138. 2019. DOI: 10.1007/s00422-018-0784-8.
- [23] M. S. Olufsen, J. T. Ottesen. A practical approach to parameter estimation applied to model predicting heart rate regulation. *J Math Biol* 67 (1): 39–68. 2013. DOI: 10.1007/s00285-012-0535-8.
- [24] S. R. Pope, L. M. Ellwein, C. Zapata, V. Novak, C. T. Kelley, M. S. Olufsen. Estimation and identification of parameters in a lumped cerebrovascular model. *Math Biosci Eng* 6 (1): 93–115. 2009. DOI: 10.3934/mbe.2009.6.93.
- [25] M. U. Qureshi, M. J. Colebank, L. M. Paun, L. Ellwein Fix, N. Chesler, M. A. Haider, N. A. Hill, D. Husmeier, M. S. Olufsen. Hemodynamic assessment of pulmonary hypertension in mice: a model-based analysis of the disease mechanism. *Biomech Model Mechanobiol* 18 (1): 219–243. 2019. DOI: 10.1007/s10237-018-1078-8.
- [26] E. B. Randall, A. Billeschou, L. S. Brinth, J. Mehlsen, M. S. Olufsen. A model-based analysis of autonomic nervous function in response to the Valsalva maneuver. *J Appl Physiol* 127 (5): 1386–1402. 2019. DOI: 10.1152/jappphysiol.00015.2019.
- [27] E. B. Randall, N. Z. Randolph, M. S. Olufsen. Persistent instability in a nonhomogeneous delay differential equation system of the Valsalva maneuver. *Math Biosci* 319: 108292. 2019. DOI: 10.1016/j.mbs.2019.108292.
- [28] E. B. Randall. Time-varying global sensitivity analysis software (Version 2.1) [Computer software]. DOI: 10.5281/zenodo.4382698.
- [29] A. Saltelli, P. Annoni, I. Azzini, F. Campolongo, M. Ratto, S. Tarantola. Variance based sensitivity analysis of model output. Design and estimator for total sensitivity index. *Comput Phys Commun* 181 (2): 259–270. 2010. DOI: 10.1016/j.cpc.2009.09.018.
- [30] R. C. Smith. *Uncertainty quantification: theory, implementation, and applications*. Society for Industrial and Applied Mathematics (SIAM), Philadelphia, PA. 2014. ISBN: 978-1611973211.
- [31] T. J. Snowden, P. H. van der Graaf, M. J. Tindall. Model reduction in mathematical pharmacology. *J Pharmacokinetic Pharmacodyn* 45 (4): 537–555. 2018. DOI: 10.1007/s10928-018-9584-y.
- [32] I. M. Sobol. Sensitivity estimates for nonlinear mathematical models. *Math Mod Comp Exp* 1 (4): 407–414. 1993.
- [33] I. M. Sobol. Global sensitivity indices for nonlinear mathematical models and their Monte Carlo estimates. *Math Comput Simul* 55 (1-3): 271–280. 2001. DOI: 10.1016/S0378-4754(00)00270-6.
- [34] I. M. Sobol, S. S. Kucherenko. Derivative based global sensitivity measures. *Procedia Soc Behav Sci* 2 (6): 7745–7746. 2010. DOI: 10.1016/j.sbspro.2010.05.208.
- [35] C. B. Storlie, J. C. Helton. Multiple predictor smoothing methods for sensitivity analysis: description of techniques. *Reliab Eng Syst Safe* 93 (1): 28–54. 2008. DOI: j.ress.2006.10.012.
- [36] T. Sumner, E. Shephard, I. D. L. Bogle. A methodology for global sensitivity analysis of time-dependent outputs in systems biology modelling. *J R Soc Interface* 9 (74): 2156–2166. 2012. DOI: 10.1098/rsif.2011.0891.
- [37] E. Wit, E. ven den Heuvel, J.-W. Romeijn. ‘All models are wrong . . .’: an introduction to model uncertainty. *Stat Neerl* 66: 217–236. 2012. DOI: 10.1111/j.1467-9574.2012.00530.x.